Molecular Medicine

Alternative Mechanism for White Adipose Tissue Lipolysis after Thermal Injury

Li Diao,[1] David Patsouris,[1] Ali-Reza Sadri,[1] Xiaojing Dai,[1] Saeid Amini-Nik,[1,2] and Marc G Jeschke[1,2,3]

[1]Sunnybrook Research Institute, Toronto, Ontario, Canada; [2]Department of Surgery, Division of Plastic Surgery, Department of Immunology, University of Toronto, Toronto, Ontario, Canada; and [3]Ross Tilley Burn Center, Sunnybrook Health Sciences Center, Toronto, Ontario, Canada

Extensively burned patients often suffer from sepsis, a complication that enhances postburn hypermetabolism and contributes to increased incidence of multiple organ failure, morbidity and mortality. Despite the clinical importance of burn sepsis, the molecular and cellular mechanisms of such infection-related metabolic derangements and organ dysfunction are still largely unknown. We recently found that upon endoplasmic reticulum (ER) stress, the white adipose tissue (WAT) interacts with the liver via inflammatory and metabolic signals leading to profound hepatic alterations, including hepatocyte apoptosis and hepatic fatty infiltration. We therefore hypothesized that burn plus infection causes an increase in lipolysis of WAT after major burn, partially through induction of ER stress, contributing to hyperlipidemia and profound hepatic lipid infiltration. We used a two-hit rat model of 60% total body surface area scald burn, followed by intraperitoneal (IP) injection of *Pseudomonas Aeruginosa*-derived lipopolysaccharide (LPS) 3 d postburn. One day later, animals were euthanized and liver and epididymal WAT (EWAT) samples were collected for gene expression, protein analysis and histological study of inflammasome activation, ER stress, apoptosis and lipid metabolism. Our results showed that burn plus LPS profoundly increased lipolysis in WAT associated with significantly increased hepatic lipid infiltration. Burn plus LPS augmented ER stress by upregulating CHOP and activating ATF6, inducing NLRP3 inflammasome activation and leading to increased apoptosis and lipolysis in WAT with a distinct enzymatic mechanism related to inhibition of AMPK signaling. In conclusion, burn sepsis causes profound alterations in WAT and liver that are associated with changes in organ function and structure.

Online address: http://www.molmed.org
doi: 10.2119/molmed.2015.00123

INTRODUCTION

Major burn injury represents one of the most severe forms of trauma and features pervasive stress responses at cellular, tissue and systemic level (1,2). Such stress responses are usually followed by wound infection, systemic inflammatory responses and sepsis that augment the severity of metabolic dysfunction and immunological impairment in the patient (3). Persisting catabolic hypermetabolism, including insulin resistance (IR), hyperglycemia and lipolysis, is the common clinical manifestation in severely burned patients, and these responses are augmented when sepsis is present (4). This can lead to impaired immune function and poor wound healing, and can increase the incidence of multiple organ dysfunction/failure and even death (5,6). We have previously shown in animal models that burn injury plus lipopolysaccharide (LPS) injection induces inflammasome activation in liver, augments hepatic endoplasmic reticulum (ER) stress and liver damage, thus contributing to metabolic derangement (7). Using this model, we observed increased fatty infiltration in liver tissue. This is consistent with the clinical findings that significant hepatic fatty infiltration and hepatomegaly are associated with increased incidence of sepsis and mortality in severely burned patients (8,9); however, the mechanisms underlying the abnormal deposition of lipid in the liver are unclear. Due to the increased appreciation of metabolic cross-talk between liver and WAT in the context of IR and hypermetabolism (10), we hypothesized that increased lipolysis in WAT after severe burn injury and sepsis contributed to hyperlipidemia and hepatic lipid infiltration that led to detrimental outcomes.

The aim of the current study was to determine the underlying mechanisms of

Address correspondence to *Marc G Jeschke, Ross Tilley Burn Centre, Sunnybrook Health Sciences Centre, University of Toronto, 2075 Bayview Avenue, Room D704, Toronto, ON, Canada M4N 3M5. Phone: 416-480-6703; Fax: 416-480-6763; E-mail: marc.jeschke@sunnybrook.ca.*

Submitted May 18, 2015; Accepted for publication December 29, 2015; Published Online (www.molmed.org) December 29, 2015.

The Feinstein Institute for Medical Research
North Shore LIJ
Empowering Imagination. Pioneering Discovery.®

lipolysis postburn using a two-hit model of burn plus LPS. We also examined whether hepatic steatosis is linked to pathological changes in WAT.

MATERIALS AND METHODS

Animal Model

Animal experiments were approved by the Animal Care and Use Committee of Sunnybrook Research Institute in Toronto, Ontario. We follow the *Guide for the Care and Use of Laboratory Animals*, 2011, adopted by the National Institutes of Health (NIH).

Male Sprague Dawley rats (n = 8 per group), 275 to 300 grams, were purchased from Charles Rivers Laboratory International Inc. and were allowed to acclimate for 1 wk before experiments. Rats were housed in the Sunnybrook Research Institute animal care facility and received a high protein diet (Ensure, #22017C8, Abbott Laboratories) and water *ad libitum* from arrival until euthanization. Ensure was given from 7 d before the study to adjust the animals to the liquid diet.

The animals were randomized into four groups: sham, burn only, LPS only and burn plus LPS. A well-established method was used to induce a full-thickness scald burn of 60% total body surface area (11,12). Briefly, the animals were anesthetized with IP injection of ketamine (40 mg/kg) and xylazine (5 mg/kg), shaved on both the dorsum and the abdomen and then placed in a mold that exposed a defined area of skin. The exposed skin was lowered into water of 98°C for 10 s on the back and 1.5 s on the abdomen to induce full-thickness scald burn. Lactated Ringer solution (30 ml/kg) was administered IP immediately after the burn for resuscitation. Sham animals were anesthetized and shaved but not burned. The second hit of an IP injection of LPS from *Pseudomonas aeruginosa* (10 mg/kg, Sigma) was applied 72 h postburn. All the animals were euthanized 24 h after LPS injection (96 h postburn) (7).

Cell Culture

3T3-L1 cells were maintained in Dulbecco's modified Eagle's medium supplemented with 10% FBS, 2 mmol/LL glutamine, 100 U/mL penicillin and 100 mg/mL streptomycin in a humidified atmosphere containing 5% CO_2 at 37°C. Differentiation of the cells to mature adipocytes was performed as described previously using a differentiation cocktail containing rosiglitazone (13). Adipocytes were serum deprived overnight before the experiment. After the treatment, the cells were briefly washed with phosphate-buffered saline (PBS) and then preserved immediately at –80°C for future analysis.

Plasma and Tissue Collection

Blood was collected into EDTA-containing tubes (30 μL of 0.5 mol/L EDTA). The tubes were placed on ice for at least 30 min and centrifuged at 4°C for 10 min at 1,000*g*. The plasma supernatant was aliquoted and stored at –80°C for later analysis. Livers were collected after brief portal vein perfusion with PBS (10 mL). Liver and WAT were frozen immediately on dry ice and then stored at –80°C for gene expression and Western blot analyses. Tissue samples were fixed in 10% buffered formalin at 4°C overnight, transferred to 70% ethanol and then paraffin embedded for histology. A second set of tissue samples were embedded in OCT compound (VWR Cat No: 95057-838), frozen on dry ice and stored at –80°C for oil red O (ORO) staining.

Gene Expression Analysis

Total RNA was isolated from liver following manufacturer's instructions (RNeasy Mini Kit; Qiagen), quantified using a Nanodrop spectrophotometer (NanoDrop Technologies) and reverse transcribed (Applied Biosystems). Real-time quantitative PCR was performed on cDNA with the housekeeping gene rRNA 18S. The sequences of primers of ER stress marker gene CCAAT/-enhancer-binding protein homologous protein (*Chop*): 5′-AGCGC CTGAC CAGGG AGGTA-3′ and 5′-GCTTG GCACT GGCGT GATGG T-3′.

Western Blotting

Antibodies against rat total and phosphorylated AMP-activated protein kinase (AMPKα and phospho-AMPKα), total and phosphorylated protein kinase A catalyst unit (PKA C and phospho-PKA C), hormonal-sensitive lipase (HSL, total and phosphorylated at Ser563, 565, 660 respectively), phosphorylated p44/42 MAPK, perilipin, CHOP, caspase-3, caspase-9, cleaved caspase-3, cleaved caspase-7, GAPDH and tubulin were Cell Signaling products. Anti-NOD-like receptor, pyrin domain containing 3 (NLRP3) and anti-ATF6 antibodies were EMD Millipore products. SuperSignal West Pico Chemiluminescent Substrate was a Thermo Scientific Inc. product.

WAT homogenates and whole cell lysates (50 μg of protein per well) were separated by 10% SDS-PAGE gel, proteins were transferred to nitrocellulose membrane as described previously (7) and then blots were probed using the antibodies listed above. Band intensities were detected, normalized and quantified with the Chemidoc and Image Lab 5.0 software (Bio-Rad Laboratories). GAPDH and tubulin were used as loading controls depending on molecular weights of the target proteins.

Immunofluorescent Multichannel Staining of WAT

Antibody staining was performed as described previously (14). Primary antibodies against perilipin, cleaved caspase-3 and CHOP were Cell Signaling products. Fluorophore secondary antibodies (Alexa Fluor 647 Donkey Anti-Mouse and Alexa Fluor 488 Goat Anti-Rabbit) were Life Technologies products. Multiple negative controls of blank, first or second antibodies alone were set up in each batch of experiment to deduct the autofluorescence of the WAT. Mounting media with DAPI was applied for nuclear staining. The percentage of marker-positive cells was determined by taking representative images and directly counting cell numbers. Cell enumerations for each experiment are listed in the text or figure legends.

Hematoxylin and Eosin (H&E), ORO, Immunohistochemical (IHC) and TUNEL Staining of Tissue Sections

H&E and ORO staining of WAT as well as IHC staining of perilipin in liver were performed as described previously (15,16). The size of adipocytes was measured using ImageJ v1.48 (NIH). TUNEL staining of WAT was performed using an immunofluorescent TUNEL staining kit following the manufacturer's instructions (Promega).

Determination of Free Fatty Acid (FFA), Glycerol and Triglyceride Levels in Blood

Levels of FFA, glycerol and triglyceride in the blood were determined using FFA, glycerol and triglyceride colorimetric assay kits according to the manufacturer's instructions (Cayman Chemical).

Statistical Analysis

The statistical analysis was performed using Prism version 5.01 (GraphPad Software). $P < 0.05$ was considered statistically significant.

All supplementary materials are available online at www.molmed.org.

RESULTS

Burn and LPS Induce Significant Catabolism and Hepatic Fatty Infiltration

We observed significant weight loss in the LPS and the burn plus LPS groups compared with the sham controls, but there were no changes in body weight in the animals subjected to burn alone (Figure 1A). IHC staining of perilipin and ORO staining of neutral lipid in liver indicated increased lipid accumulation in the burn and LPS groups; however, we observed a synergistic effect of burn plus LPS on perilipin and neutral lipid in liver (Figures 1B–E). Observation of increased hepatic steatosis corroborates previous findings and validates our two-hit animal model, implicating catabolism and robust lipid mobilization from WAT after burn plus LPS.

Increased WAT Lipolysis in the Two-Hit Rat Model of Burn plus LPS

We found lower EWAT mass (data not shown) as well as a smaller median

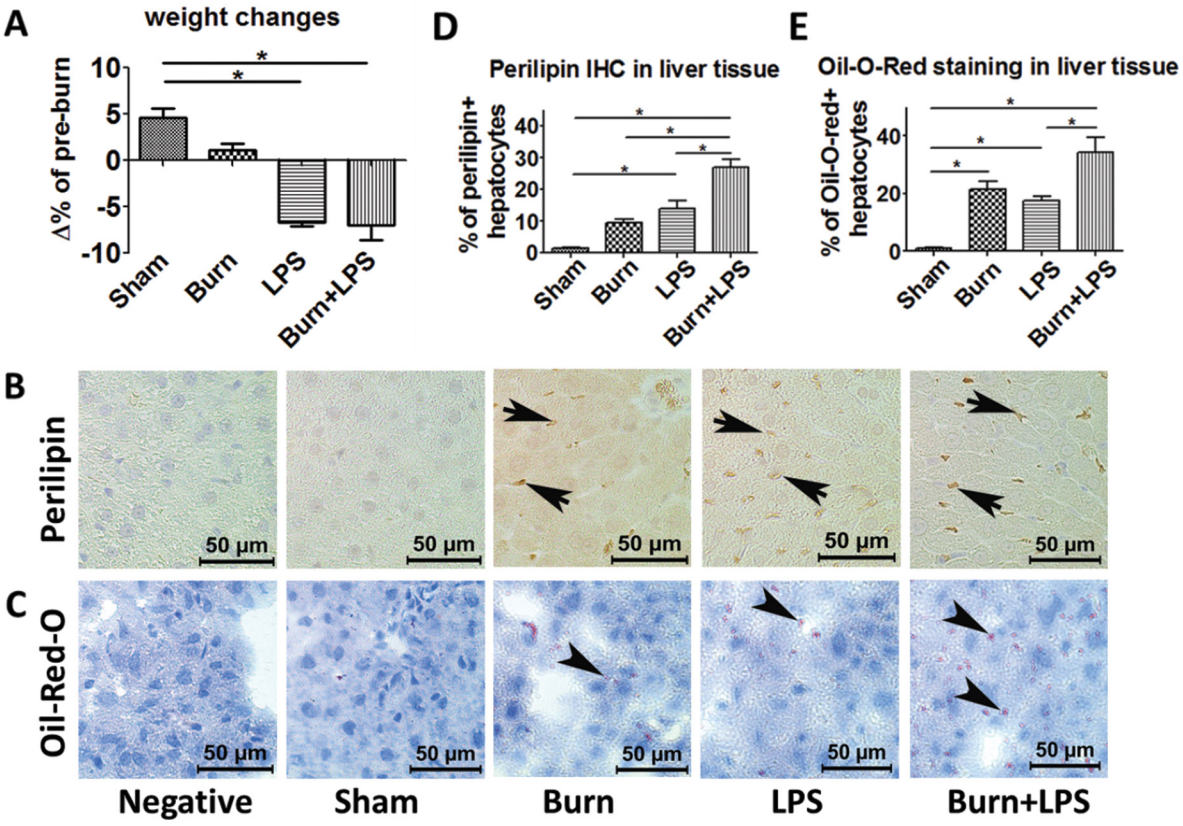

Figure 1. Burn and LPS induced catabolism and increased liver fat content. (A) Weight gain/loss presented is in percentage of preexperimental weight. (B) Representative images of perilipin IHC in liver. Arrows indicate perilipin staining. Scale bar = 50 μm. (C) Representative images of ORO staining of liver. Arrowheads indicate positive ORO staining. Scale bar = 50 μm. (D–E) Percentage of perilipin-positive and ORO-positive hepatocytes. Values are means ± SEM. *$P < 0.05$ (one-way ANOVA, Bonferroni posttest). N = 8 animals per group, N = 2 for histological observations in each group.

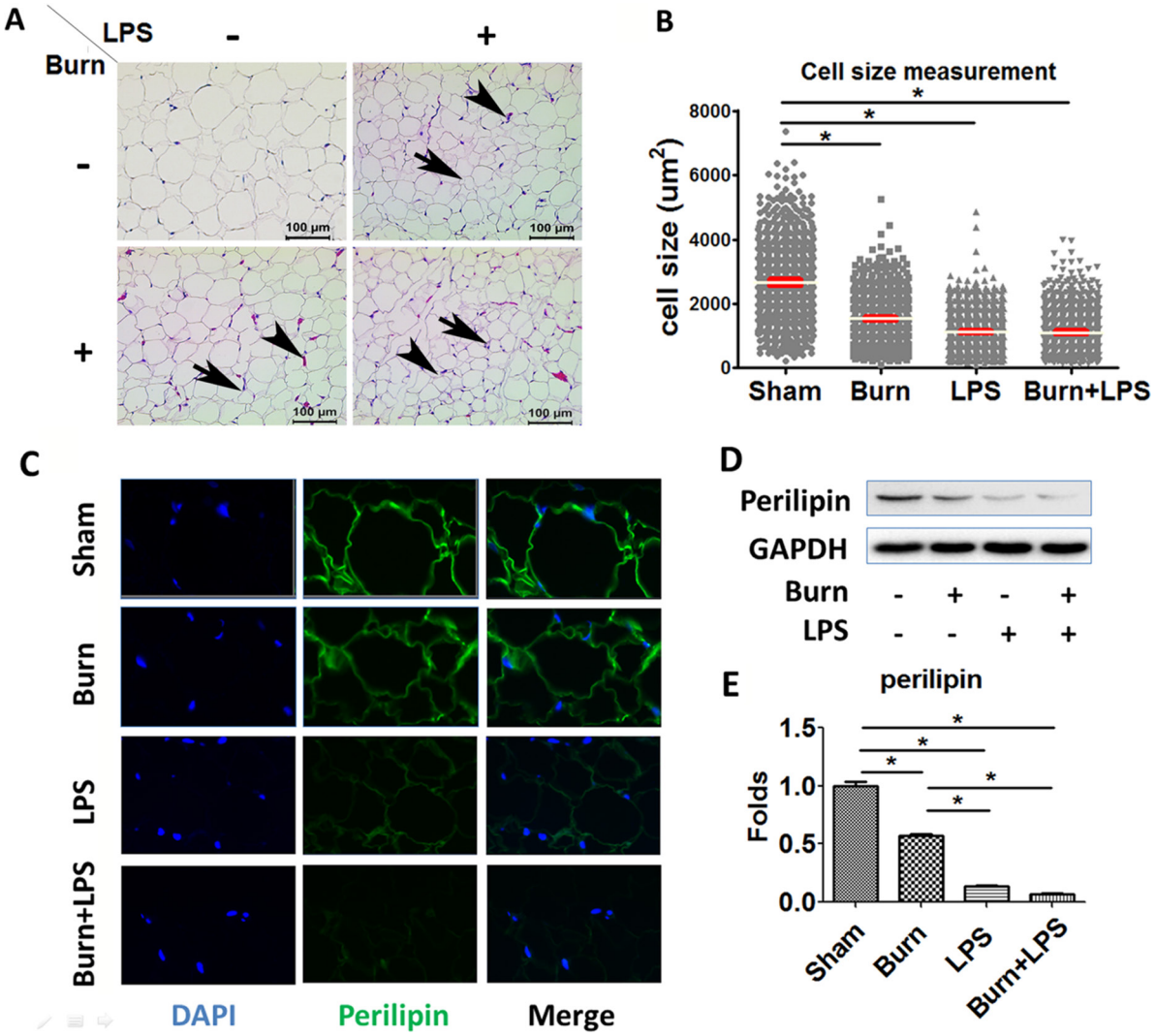

Figure 2. Decreased adipocyte cell size and perilipin content in WAT of rats subjected to burn plus LPS. (A) Representative images depict H&E staining of EWAT. Arrows indicate smaller adipocytes in burn, LPS and burn plus LPS as compared with sham; arrowheads indicate cell infiltration in WAT. Scale bar = 100 μm. (B) Measurement of adipocyte cell size, 1000 cells per group. Values are means ± SEM (shown in brown and red bars). *P < 0.05 (one-way ANOVA, Bonferroni posttest). (C) Immunofluorescent staining of perilipin in EWAT (magnification 400×). (D–E) Representative images of Western blot and quantitative densitometric analyses for perilipin in EWAT. Values are means ± SEM, *P < 0.05 (one-way ANOVA, Bonferroni posttest). N = 8 animals per group, N = 2 for histological observations in each group.

adipocyte cell size in burn, LPS and burn plus LPS groups compared with sham (Figure 2A). The median adipocyte size in sham animals was 2500 μm^2, whereas 90% of adipocytes in burn, LPS and burn plus LPS groups were smaller than 2500 μm^2 (Figure 2B). Furthermore, immunofluorescent staining of WAT sections (Figure 2C) and Western blot analysis of WAT (Figures 2D, E) demonstrated that the perilipin coating of adipocytes in burn, LPS and burn plus LPS animals was significant compared with sham, supporting the notion that WAT lipolysis was exacerbated in the two-hit rat model (17).

Increased Lipolysis in WAT after Burn plus LPS Is Associated with Reduced AMPK Signaling

To explore potential mechanisms of increased lipolysis in WAT after burn plus LPS, we explored the activation of HSL and MAPK. Unexpectedly, Western blot analysis showed that lipolysis-related phosphorylation of HSL at Ser563 and Ser660 did not increase in burn or LPS groups and, in fact, decreased in the burn plus LPS group. The other lipolysis-related phosphorylation of MAPK at Thr202/Tyr204 and Thr185/Tyr187 also decreased in burn, LPS and burn plus LPS groups. These data are consistent with the

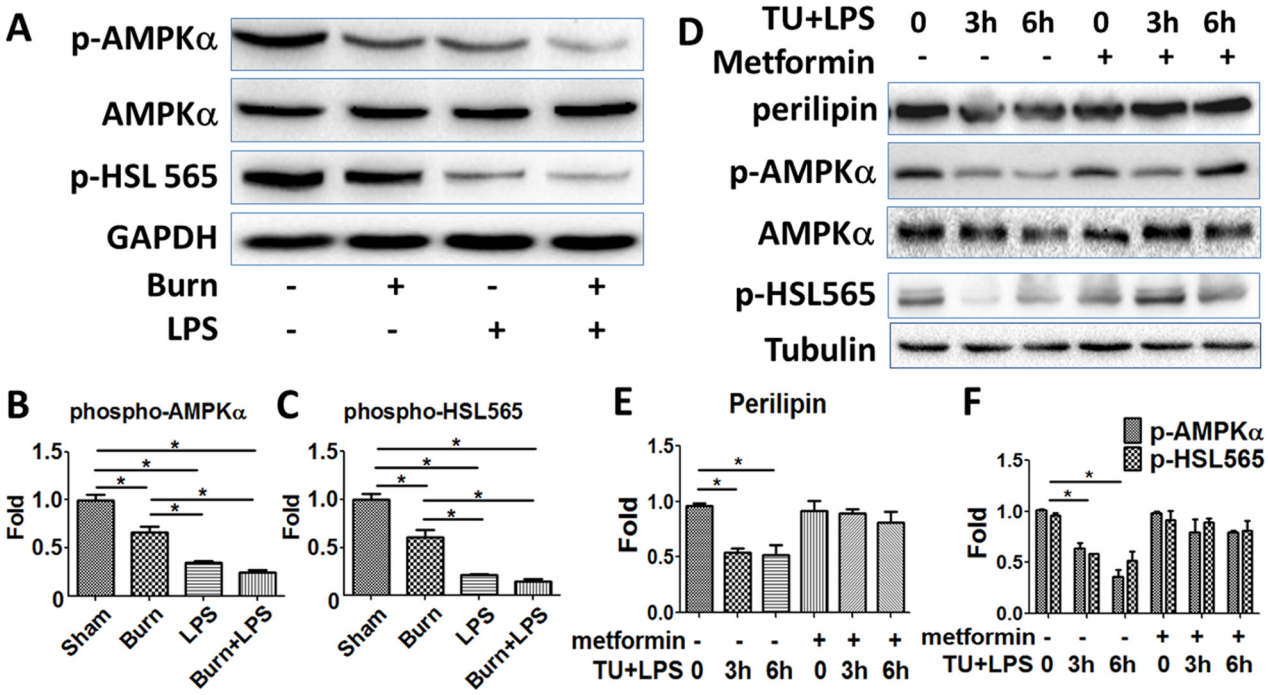

Figure 3. Burn and LPS increased lipolysis by inhibiting AMPK signaling in WAT. (A) Representative images of Western blot for phosphorylation of HSL at Ser565 and its upstream modulator of AMPK in WAT. (B–C) Quantitative densitometric analyses for Western blots in (A) Values are means ± SEM. N = 8 animals in each group. *$P < 0.05$ (one-way ANOVA, Bonferroni posttest). (D) Representative images of Western blots for perilipin, phospho-AMPK and phospho-HSL (Ser565) in *in vitro* differentiated 3T3-L1 adipocytes with or without pretreatment of 1 mmol/L metformin for 6 h and then challenged by 5 μg/mL tunicamycin and 100 ng/mL LPS for 3 or 6 h, respectively. (E–F) Quantitative densitometric analyses for Western blots in (D). Values are means ± SEM. *$P < 0.05$ (one-way ANOVA, Bonferroni posttest). *In vitro* experiments on 3T3-L1 adipocytes were repeated 3 times.

inhibition of their upstream modulator, PKA (Supplementary Figures 1A–E). Increased lipolysis is thus attributed to the suppression of inhibitory phosphorylation of HSL at Ser565 as the result of suppression of its upstream regulator AMPK (Figures 3A–C). Indeed, using well-differentiated 3T3-L1 adipocytes, we confirmed that the stimulation of lipolysis by ER stress and LPS challenge occurs via suppression of AMPK and HSL phosphorylation at Ser565. We also showed that such lipolysis could be rescued by the AMPK agonist metformin (Figures 3D, F) and AICAR (data not shown).

Burn plus LPS Increases Adipocyte Apoptosis

To determine if apoptosis was contributing to increased lipolysis after burn plus LPS, we performed TUNEL staining on WAT sections (Figure 4A). Burn and LPS individually and synergistically increased adipocyte apoptosis in WAT (Figure 4B), and this correlated with lipid content of the liver (Figure 4C). We also found that burn plus LPS stimulated proapoptotic signals, shown by the significant increase of caspase-9, caspase-3, cleaved caspase-3 and cleaved caspase-7 in WAT (Figures 4D–H).

Burn and LPS Synergistically Induce Apoptosis in WAT

Apoptosis is associated with ER stress predominantly through transcription factor CHOP (18). We found significantly higher expression of *Chop* mRNA (Figure 5A) and protein (Figures 5B, C) in burn, LPS and burn plus LPS compared with sham. The protein levels of ATF6 and cleaved ATF6 also were significantly higher in burn, LPS and burn plus LPS (Figures 5B, D, E). CHOP colocalized with the proapoptotic marker cleaved caspase-3 in double immunofluorescent staining (Figures 5F, G). While burn alone increased the number of cells with ER stress, LPS predominately increased the apoptotic responses. A synergistic effect was observed in the burn plus LPS group (Supplementary Figures 2B–F).

Increased Macrophage Infiltration and Inflammasome Activation Correlated with Apoptosis in WAT

Western blot analyses of NLRP3, caspase-1 and IL-1β in WAT demonstrated that the NLRP3 inflammasome was activated in burn plus LPS animals (Figures 6A–D). Immunofluorescent double staining showed colocalization of the macrophage marker MAC387 (19) and proapoptotic marker cleaved caspase-3 (Figures 6E, F),

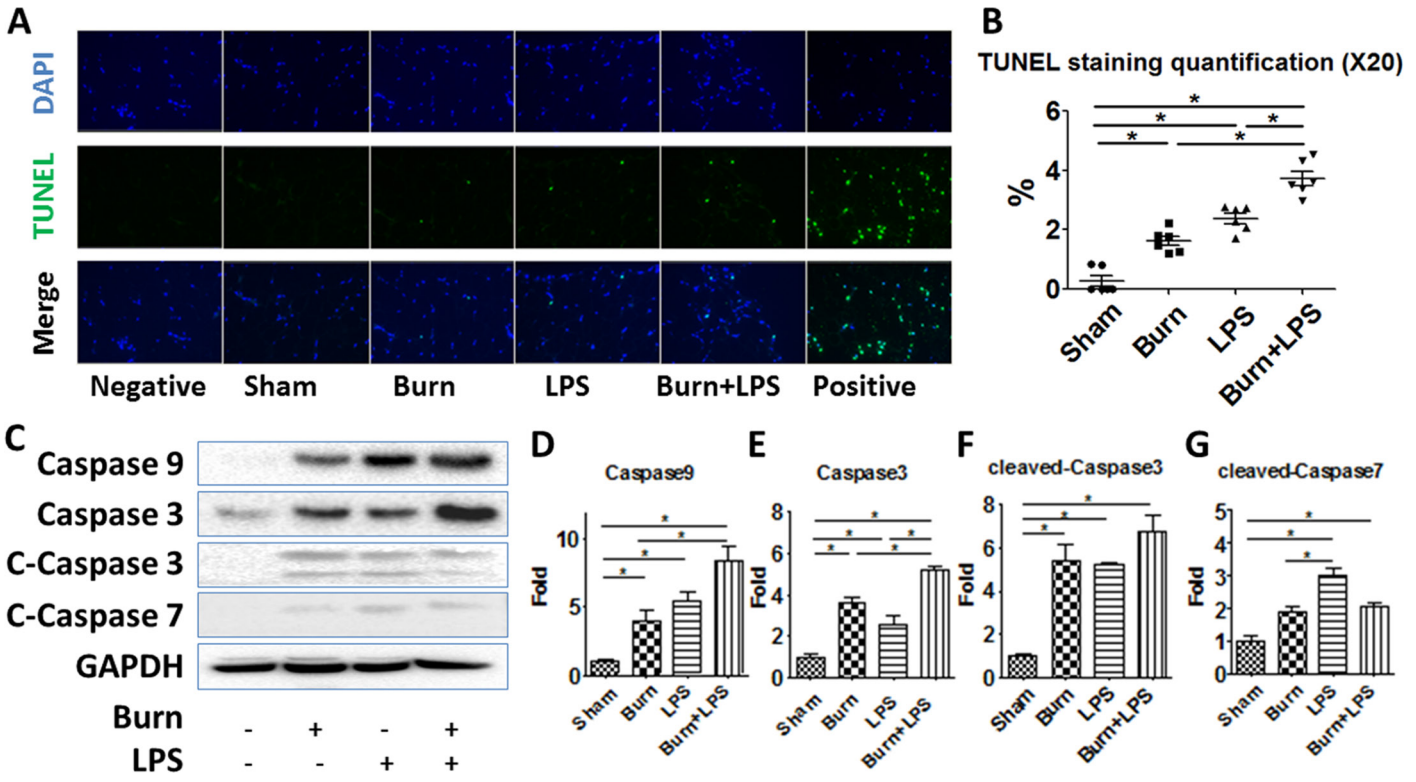

Figure 4. Burn plus LPS promoted apoptosis in WAT. (A) Representative images of immunofluorescent TUNEL staining of EWAT. Arrows indicate TUNEL-positive cells (magnification 200×). (B) Quantitative analysis of positive TUNEL-staining cells in EWAT. Values are means ± SEM. $P < 0.05$ in each paired comparison between groups except that between burn and LPS only (one-way ANOVA, Bonferroni posttest). (C) Correlate coefficient analysis between percentage of ORO-positive hepatocytes and percentage of TUNEL-positive cells in WAT. (D) Representative images of Western blots for proapoptotic signaling molecules including caspase-9, caspase-3, cleaved-caspase-3 and cleaved caspase-7. (E–H) Quantitative densitometric analyses for the above Western blots. Values are means ± SEM. *$P < 0.05$ (one-way ANOVA, Bonferroni posttest). N = 8 animals per group, N = 2 for histological observations in each group.

suggesting that WAT macrophages were undergoing apoptosis. Burn, LPS and burn plus LPS increased WAT macrophage (MAC387-positive cells) infiltration (Supplementary Figure 3B), while LPS and burn plus LPS further stimulated macrophage apoptosis (Supplementary Figures 3C, D). There also was a significant increase in adipocytic (MAC387 negative cells) and overall apoptosis in the burn plus LPS group (Supplementary Figures 3E, F).

DISCUSSION

Using the rat two-hit model of severe burn injury followed by LPS IP injection, we mimicked the clinical scenario of burn followed by sepsis and investigated the lipid metabolism cross-talk between WAT and liver during critical illness. We found that there is significant more WAT lipolysis and hepatic fatty infiltration in burn plus LPS compared with burn alone. Mechanistically, we attribute the enhanced lipolysis in WAT mainly to the degradation of the perilipin coating of the lipid droplet and to the impairment of AMPK signaling as well as its downstream lipolysis-inhibiting HSL phosphorylation at Ser565. We also found that augmented ER stress, NLRP3 inflammasome activation and apoptosis converged to enhance WAT lipolysis under conditions of severe acute stress.

WAT and liver are in constant communication with one another. For example, JNK1 activation in WAT causes diet-induced hepatic IR (20). Moreover, inhibition of hepatic eIF2α (involved in protein synthesis and ER stress) impairs WAT insulin sensitivity (21). In the current study, we demonstrated that increased WAT apoptosis is positively correlated with lipid infiltration in the liver, implicating increased WAT lipolysis as a source of lipid for deposition in the liver. While this partly explains the morphologic changes in the liver after severe burn, further investigation is needed to determine the mechanisms underlying pronounced hepatic steatosis following thermal injury. It is also possible that decreased fatty acid oxidation and outbound lipid transportation due to impaired hepatocyte function contribute to increased fat content in the liver.

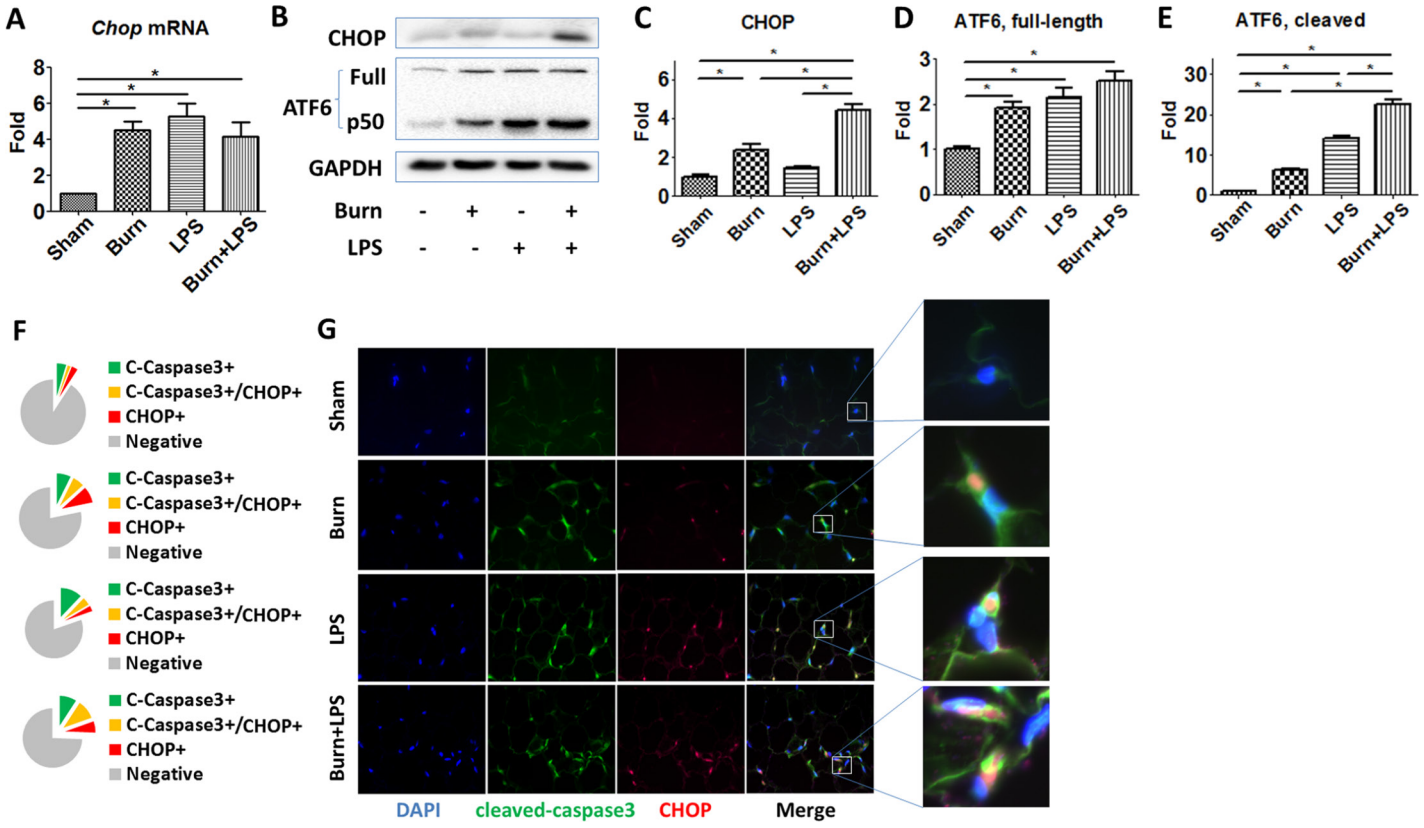

Figure 5. Burn plus LPS increased ER stress, which correlated with apoptosis in WAT. (A) RT-qPCR analysis of mRNA levels of *Chop* in EWAT. RT-qPCR data were normalized to 18s rRNA as an internal control. Values are means ± SEM. **P* < 0.05 (one-way ANOVA, Bonferroni posttest). (B) Representative images of Western blots for ER stress markers (CHOP, ATF6) in WAT. (C–E) Quantitative densitometric analyses for the above Western blots. Values are means ± SEM. **P* < 0.05 (one-way ANOVA, Bonferroni posttest). (F) Immunofluorescent double staining of cleaved caspase-3) and CHOP in WAT (magnification 400×). Arrows indicate CHOP positive cells. Arrowheads indicate cleaved caspase-3 positive cells. (G) Percentage of immunofluorescent positive cells in WAT in each treatment group. N = 8 animals per group, N = 2 for histological observations in each group.

Interestingly, we did not observe a significant elevation of circulating FFA, glycerol or triglycerides in burn, LPS or burn plus LPS groups (Supplementary Figure 4). There are two possible explanations for this. First, plasma lipid concentration represents an equilibrium between what is released and what is taken up and thus may not reflect the changes in flux (22), as is indicated in high fat-fed mice which exhibit no significant increases in blood FFA or glycerol (23). Secondly, considering the severity of the intervention of burn plus LPS, we did not fast the animals before collecting the blood samples. Differences in food intake of the animals would significantly affect the plasma FFA, glycerol and triglyceride levels. Nonetheless, the correlation of TUNEL staining in WAT and ORO staining in liver suggests that increased lipolysis in WAT contributes to the lipid infiltration in the liver. Hepatic steatosis contributes to augmented hepatic ER stress, mitochondrial dysfunction and insulin resistance (24,25). Moreover, it may impair the hepatic clearance of LPS (26). As shown in the current animal study and in other clinical observations (17,27), LPS strongly activates lipolysis in WAT, which could instigate a vicious positive feedback loop between WAT lipolysis, hepatic lipid accumulation and hepatic LPS clearance.

As a mechanism of energy reservation and buffering, lipolysis of WAT is regulated by multiple signaling pathways (28,29). The first step of lipid mobilization from WAT is the phosphorylation or degradation of perilipin and activation of desnutrin/adipose triglyceride lipase (ATGL), which converts triacylglycerol (TAG) to diacylglycerol (DAG). Activated HSL then converts DAG into 2-monoacylglycerol (MAG), which, in turn, is broken down by monoacylglycerol lipase (MGL) into FFA and glycerol. HSL can convert TAG to DAG and has long been considered the key regulator of lipolysis and its activation the driving force for hyperlipidemia since MGL is abundant and its catalyzing activity is not rate-limited (30). This is true in low-grade, chronic adipose stress conditions such

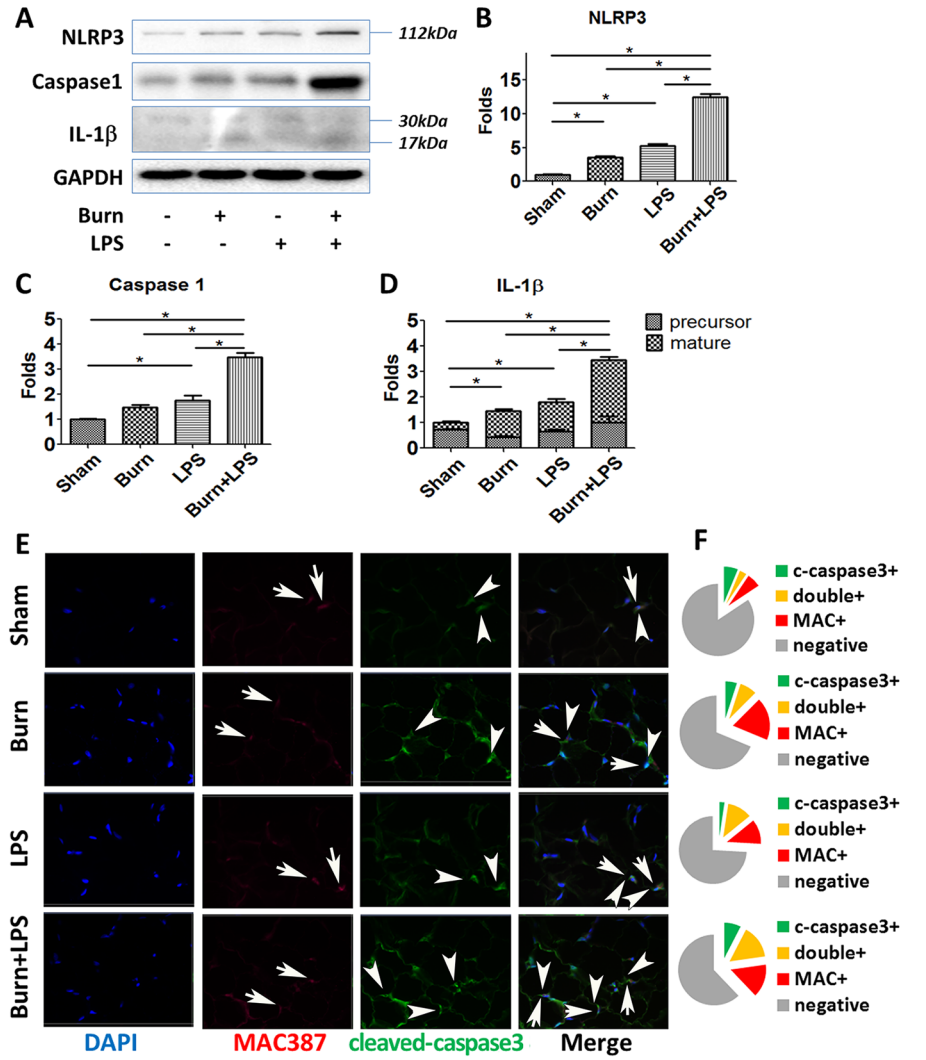

Figure 6. Burn and LPS stimulated macrophage infiltration and inflammasome activation, which correlated with apoptosis in WAT. (A) Representative images of Western blots for NLRP3, caspase-1 and IL-1β in WAT. (B–D) Quantitative densitometric analysis for Western blot of NLRP3, caspase-1 and IL-1β in WAT. Values are means ± SEM. *$P < 0.05$ (one-way ANOVA, Bonferroni posttest). For IL-1β, P value was calculated for 17 kDa mature form. (E) Immunofluorescent double staining of cleaved caspase-3 and MAC387 in WAT (magnification 400×). Arrows indicate MAC387 positive cells. Arrowheads indicate cleaved caspase-3 positive cells. (F) Percentage of immunofluorescent positive cells in WAT in each treatment group. N = 8 animals per group, N = 2 for histological observations in each group.

as obesity and diabetes, where increased lipolysis occurs in parallel to activation of PKA and HSL phosphorylation at Ser563, Ser660 (31). Based on our observations, HSL and its upstream modulators PKA and MAPK were all suppressed under severe and acute traumatic stress conditions, yet we still observed augmented lipolysis and even more severe ectopic lipid deposition in liver. In the current study, we demonstrated that the inhibition of AMPK and its downstream phosphorylation of HSL at Ser565 contribute to activation of lipolysis in WAT under severe stress conditions.

We also observed increased apoptosis in WAT, which has been implicated in the enhancement of lipolysis (32). To address the causative factors of increased apoptosis, we first determined whether there was augmented ER stress in WAT after burn plus LPS since it is well accepted that ER stress triggers apoptosis under multiple circumstances (32,33). Here, we showed that burn injury alone significantly induces ER stress in WAT. Together with LPS-mediated proapoptotic signaling, burn plus LPS further stimulated ER stress and apoptosis, as shown by the robust activation of apoptosis-related ER stress markers CHOP and ATF6 as well as enhanced TUNEL staining. Changes in the proapoptotic signaling indicated that ER stress induced by burn injury mainly activated the intrinsic pathway of apoptosis that is manifested by activation of caspase-9 and increased cleavage of caspase-3 (34). Caspase-7 is a direct substrate of caspase-1, one of the products of inflammasome activation. As such, significantly increased cleavage of caspase-7 in LPS and burn plus LPS groups suggests the contribution of inflammation and inflammasome activation on apoptosis (35).

We have previously reported the activation of the inflammasome in the WAT of burn patients (36). As the WAT was collected from the wound or adjacent area in these experiments, this raises the question whether inflammasome activation also occurs in distal tissue and organs. In the current study, we observed in experimental animals that severe burn injury and LPS trigger macrophage infiltration and subsequent NLRP3 inflammasome activation in WAT distal to burn wound. It has long been postulated that the danger-associated molecular pattern molecules (DAMPs) contribute to inflammasome activation (37,38). While the identity of the DAMP(s) involved is undetermined to date, augmented ER stress may be responsible for the production of DAMPs considering the concomitance of ER stress and inflammasome activation in WAT (39). Furthermore, since the outcome of NLRP3 inflammasome activation is the maturation

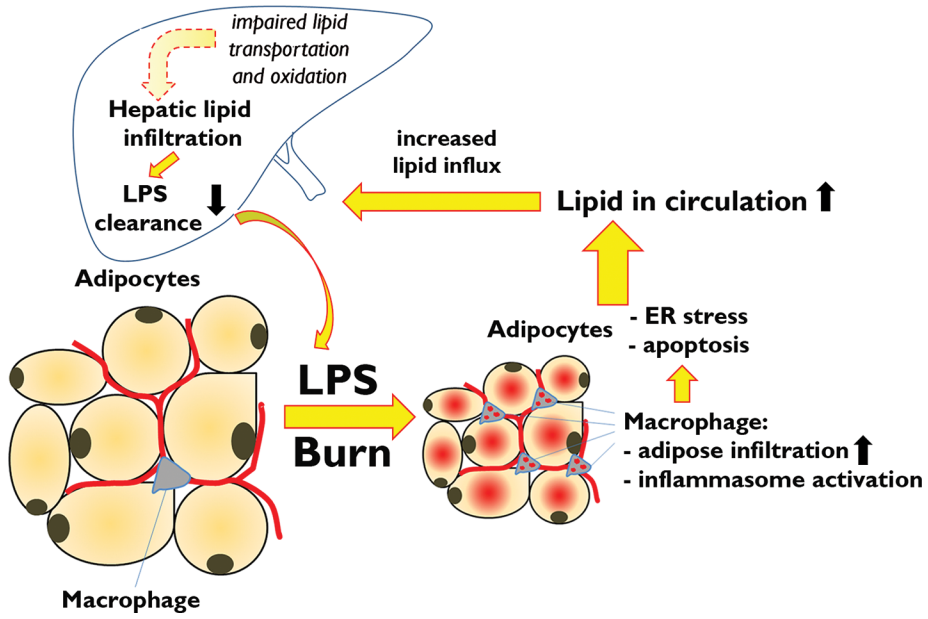

Figure 7. Increased WAT lipolysis and its hypothetical contribution to immunological and metabolic impairment in the two-hit model of burn plus LPS. In the acute phase after major trauma, such as an extensive burn, excessive DAMPs and PAMPs, which are derived from wounds, gut, homeostasis derangement and damaged tissues, redistribute to liver and WAT, induce ER stress and stimulate inflammasome activation in these tissues. ER stress and inflammasome activation in WAT contribute to apoptosis and lipolysis, releasing FFA and glycerol, which, subsequently, accumulate in the liver. Lipid deposition in the liver not only augments hepatic ER stress and impairs hepatic metabolic signaling but also inhibits LPS clearance and further stimulates the inflammasome, which perturbs hepatic immune function. In the two-hit model, LPS exacerbates impaired metabolism by stimulating both canonical WAT lipolysis and a proinflammatory response in the liver.

of proinflammatory cytokine IL-1β, which then contributes to increased lipolysis, IR and hyperglycemia, the resulting prolonged hyperglycemic response further enhances and sustains inflammasome activation and proinflammatory responses, serving as another positive feedback loop contributing to increased postburn morbidity and mortality (40,41).

CONCLUSION

In the two-hit model of burn plus LPS, ER stress and inflammasome activation contribute to increased apoptosis and lipolysis in WAT. The mechanism responsible for lipolysis following major trauma and sepsis may be related to the inhibition of AMPK signaling and is distinct from that induced by chronic inflammation. Postburn WAT lipolysis correlates with lipid infiltration in liver and may form a positive feedback loop driving the vicious cycle of posttraumatic stress response, hypermetabolism and immunological impairment in severe burn plus sepsis (Figure 7).

ACKNOWLEDGMENTS

This research was supported by the National Institutes of Health (R01-GM087285-01), Canadian Institutes of Health Research (123336), the CFI Leaders Opportunity Fund (25407) and the Health Research Grant Program. We thank Cassandra Belo for her technical assistance and proofreading. We thank Abdikarim Abdullahi for his assistance in animal experiments. We are grateful to Sheila Costford for her final proofreading and editing of the manuscript.

DISCLOSURE

The authors declare that they have no competing interests as defined by *Molecular Medicine*, or other interests that might be perceived to influence the results and discussion reported in this paper.

REFERENCES

1. Jeschke MG, *et al*. (2012) Severe injury is associated with insulin resistance, endoplasmic reticulum stress response, and unfolded protein response. *Ann. Surg*. 255:370–8.
2. Jeschke MG, Boehning D. (2012) Endoplasmic reticulum stress and insulin resistance post-trauma: similarities to type 2 diabetes. *J. Cell. Mol. Med*. 16:437–44.
3. Jeschke MG, *et al*. (2015) Morbidity and survival probability in burn patients in modern burn care. *Crit. Care Med*. 43:808–15.
4. Jeschke MG, *et al*. (2014) Survivors versus non-survivors postburn: differences in inflammatory and hypermetabolic trajectories. *Ann. Surg*. 259:814–23.
5. Herndon DN, Tompkins RG. (2004) Support of the metabolic response to burn injury. *Lancet*. 363:1895–902.
6. Jeschke MG, *et al*. (2008) Pathophysiologic response to severe burn injury. *Ann. Surg*. 248: 387–401.
7. Diao L, *et al*. (2014) Burn plus lipopolysaccharide augments endoplasmic reticulum stress and NLRP3 inflammasome activation and reduces PGC-1alpha in liver. *Shock*. 41:138–44.
8. Jeschke MG. (2009) The hepatic response to thermal injury: is the liver important for postburn outcomes? *Mol. Med*. 15:337–51.
9. Barrow RE, *et al*. (2005) Identification of factors contributing to hepatomegaly in severely burned children. *Shock*. 24:523–8.
10. Glass CK, Olefsky JM. (2012) Inflammation and lipid signaling in the etiology of insulin resistance. *Cell Metab*. 15:635–45.
11. Herndon DN, Wilmore DW, Mason AD Jr. (1978) Development and analysis of a small animal model simulating the human postburn hypermetabolic response. *J. Surg. Res*. 25:394–403.
12. Jeschke MG, *et al*. (2011) Insulin protects against hepatic damage postburn. *Mol. Med*. 17:516–22.
13. Zebisch K, Voigt V, Wabitsch M, Brandsch M. (2012) Protocol for effective differentiation of 3T3-L1 cells to adipocytes. *Anal. Biochem*. 425:88–90.
14. Amini-Nik S, *et al*. (2014) Beta-catenin-regulated myeloid cell adhesion and migration determine wound healing. *J. Clin. Invest*. 124:2599–610.
15. Arno AI, *et al*. (2014) Effect of human Wharton's jelly mesenchymal stem cell paracrine signaling on keloid fibroblasts. *Stem Cells Transl. Med*. 3:299–307.

16. Bogdanovic E, *et al*. (2015) Endoplasmic reticulum stress in adipose tissue augments lipolysis. *J. Cell. Mol. Med*. 19:82–91.
17. Grisouard J, *et al*. (2012) Both inflammatory and classical lipolytic pathways are involved in lipopolysaccharide-induced lipolysis in human adipocytes. *Innate Immun*. 18:25–34.
18. Han J, *et al*. (2013) ER-stress-induced transcriptional regulation increases protein synthesis leading to cell death. *Nat. Cell Biol*. 15:481–90.
19. Yu TS, *et al*. (2010) The cannabinoid receptor type 2 is time-dependently expressed during skeletal muscle wound healing in rats. *Int. J. Legal Med*. 124:397–404.
20. Smith B, George J. (2009) Adipocyte-hepatocyte crosstalk and the pathogenesis of nonalcoholic fatty liver disease. *Hepatology*. 49:1765–7.
21. Birkenfeld AL, *et al*. (2011) Influence of the hepatic eukaryotic initiation factor 2alpha (eIF2alpha) endoplasmic reticulum (ER) stress response pathway on insulin-mediated ER stress and hepatic and peripheral glucose metabolism. *J. Biol. Chem*. 286:36163–70.
22. Bradbury MW. (2006) Lipid metabolism and liver inflammation. I. Hepatic fatty acid uptake: possible role in steatosis. *Am. J. Physiol. Gastrointest. Liver Physiol*. 290:G194–8.
23. Baranowski M, Blachnio-Zabielska A, Zabielski P, Gorski J. (2008) Pioglitazone induces lipid accumulation in the rat heart despite concomitant reduction in plasma free fatty acid availability. *Arch. Biochem. Biophys*. 477:86–91.
24. Kidani Y, Bensinger SJ. (2012) Liver X receptor and peroxisome proliferator-activated receptor as integrators of lipid homeostasis and immunity. *Immunol. Rev*. 249:72–83.
25. Palasciano G, *et al*. (2007) Non-alcoholic fatty liver disease in the metabolic syndrome. *Curr. Pharm. Des*. 13:2193–8.
26. Walley KR, *et al*. (2014) PCSK9 is a critical regulator of the innate immune response and septic shock outcome. *Sci. Transl. Med*. 6:258ra143.
27. Szalowska E, *et al*. (2011) Comparative analysis of the human hepatic and adipose tissue transcriptomes during LPS-induced inflammation leads to the identification of differential biological pathways and candidate biomarkers. *BMC Med Genomics*. 4:71.
28. Lampidonis AD, Rogdakis E, Voutsinas GE, Stravopodis DJ. (2011) The resurgence of Hormone-Sensitive Lipase (HSL) in mammalian lipolysis. *Gene*. 477:1–11.
29. Jaworski K, Sarkadi-Nagy E, Duncan RE, Ahmadian M, Sul HS. (2007) Regulation of triglyceride metabolism. IV. Hormonal regulation of lipolysis in adipose tissue. *Am. J. Physiol. Gastrointest. Liver Physiol*. 293:G1–4.
30. Zechner R, *et al*. (2012) FAT SIGNALS—lipases and lipolysis in lipid metabolism and signaling. *Cell Metab*. 15:279–91.
31. Deng J, *et al*. (2012) Lipolysis response to endoplasmic reticulum stress in adipose cells. *J. Biol. Chem*. 287:6240–9.
32. Yasuhara S, *et al*. (2006) Adipocyte apoptosis after burn injury is associated with altered fat metabolism. *J. Burn Care Res*. 27:367–76.
33. Asai A, *et al*. (2007) Primary role of functional ischemia, quantitative evidence for the two-hit mechanism, and phosphodiesterase-5 inhibitor therapy in mouse muscular dystrophy. *PLoS One*. 2:e806.
34. Siegel RM. (2006) Caspases at the crossroads of immune-cell life and death. *Nat. Rev. Immunol*. 6:308–17.
35. Lamkanfi M, Kanneganti TD. (2010) Caspase-7: a protease involved in apoptosis and inflammation. *Int. J. Biochem. Cell Biol*. 42:21–4.
36. Stanojcic M, *et al*. (2014) Leukocyte infiltration and activation of the NLRP3 inflammasome in white adipose tissue following thermal injury. *Crit. Care Med*. 42:1357–64.
37. Franchi L, Eigenbrod T, Munoz-Planillo R, Nunez G. (2009) The inflammasome: a caspase-1-activation platform that regulates immune responses and disease pathogenesis. *Nat. Immunol*. 10:241–7.
38. Martinon F, Mayor A, Tschopp J. (2009) The inflammasomes: guardians of the body. *Annu. Rev. Immunol*. 27:229–65.
39. Sasaki K, Yoshida H. (2015) Organelle autoregulation-stress responses in the ER, Golgi, mitochondria and lysosome. *J. Biochem*. 157:185–95.
40. Benetti E, Chiazza F, Patel NS, Collino M. (2013) The NLRP3 Inflammasome as a novel player of the intercellular crosstalk in metabolic disorders. *Mediators Inflamm*. 2013:678627.
41. Schroder K, Zhou R, Tschopp J. (2010) The NLRP3 inflammasome: a sensor for metabolic danger? *Science*. 327:296–300.

Cite this article as: Diao L, *et al*. (2015) Alternative mechanism for white adipose tissue lipolysis after thermal injury. *Mol. Med*. 21:959–68.